Night Operation of a Solar Chimney Integrated with Spiral Heat Exchanger

Amel Dhahri, Ahmed Omri, and Jamel Orfi

Abstract Solar power is one of the most raising and encouraging renewable source of energy generation. Solar plants are playing an important role in power supplies worldwide. Nowadays, the electrical energy demand is increasing rapidly due to fast-growing daily requirements. In the last few decades, scientific researchers have focused on a novel technology called the solar chimney power plant, sometimes recognized as solar updraft tower. The solar chimney is principally composed of three main constituents, namely, a solar collector, a chimney and a wind turbine. This promising technology addresses a very challenging idea of generating electricity from free solar energy. It is categorized as a viable resource of clean energy for many non developed countries. The world's first solar chimney prototype was designed and constructed at Manzanares in Spain, as a result of a joint project between the Schlaich Bergermann partner and the Spanish government. The plant is *characterized* by a tower high 195 m with a radius of 5 m. The radius and height of the collector encircling the tower are respectively 120 m and 1.85 m. The spanish prototype built by the engineer Jorg Schlaich of Schlaich Bergermann operated without significant problems for seven years. *Several research projects* have been conducted all *over the world* to design and introduce different solar towers based on experience gained from operating the 50 kW Spanish prototype. To ensure that the energy conversion is maintained at satisfactory levels to guarantee considerable power generation, an unprecedentedly high tower and an immense collector area are needed. This plant is then based on a thermal updraft movement of hot air resulting from *natural convection*. In this chapter, the simulations were conducted using cylindrical coordinate

A. Dhahri (✉) · A. Omri
Research Unit: Materials, Energy and Renewable Energies, College of Sciences, University of Gafsa, Gafsa, Tunisia
e-mail: dhahriamel001@yahoo.fr

A. Omri
e-mail: ahom206@yahoo.fr

J. Orfi
Department of Mechanical Engineering, King Saud University, Riadh, Saudi Arabia
e-mail: orfi@ksu.edu.sa

system. The inner fluid flow is considered turbulent and simulated with the k-ε turbulent model, by means of the CFD commercial software ANSYS Fluent. Numerical data were validated by comparing them with those from experiments. The agreement between *simulation results* and the *measurements* taken from the *experimental* plant in *Manzanares* is fairly *good*. A set of mathematical models of the solar updraft power plant have been developed where a model considering the kinetic energy difference within the solar collector was proposed. The operation of such a plant is strongly dependent on the amount of solar radiation. The main disadvantage of this system is the inability to operate constantly at night. A geothermal heating device is suggested to guarantee a continuous operation during night hours. In this chapter, an auxiliary heating system constructed of in-plane spiral coil tubes is proposed to be placed above the ground under the collector. Thus, the computational model is afterward combined with a mathematical model for a geothermal heat exchanger to evaluate the effect of combining both solar and geothermal energy on the plant performance. A parametric *study of the hybrid plant* is carried out. The study *focus essentially* on the impact of the collector size, the meteorological conditions as well as the effectiveness of the heat exchanger on the air flow rate, the temperature increase within the collector and the global performance of the solar-geothermal hybrid system.

Keywords Solar energy · Solar chimney · Collector · CFD · Electric power · Geothermal energy

Nomenclatures

List of symbols

A	Area (m^2)
A_{coll}	Solar collector area (m^2)
A_0	Heat transfer area per unit tube length
D_{tube}	Tube diameter (m)
C_p	Specific heat capacity (J/kg K)
G	Solar radiation (W/m^2)
h	Heat transfer coefficient ($Wm^{-2}K^{-1}$)
$\dot{m}$	Mass flow rate (kg s^{-1})
n_{tube}	Tube number
R	Collector radius (m)
T	Temperature (K)
U_i	Total heat transfer coefficient (W/m^2 K)
V	Air flow velocity (ms^{-1})

Greek symbols

λ	Thermal conductivity (W m^{-1} K^{-1})
μ	Dynamic viscosity (kg (s m)$^{-1}$)
ρ	Density (kg m^{-3})
$\tau\,\alpha$	Transmittance-absorbtance product
α	Rate of change of the radius

Subscript

c	Collector canopy
e	Environment or exterior
f	Fluid
i	Inner
m	Average
o	External
n	Turn number
r	Storage reservoir
s	Soil or Solar
w	Geothermal water
$w,\,in$	Heat exchanger inlet
$w,\,out$	Heat exchanger exit
x	Distance along tube (m)
1	Solar collector inlet
2	Solar collector exit
ΔT	Temperature rise (K)

1 Introduction

The ever present concern of humanity and the great challenge facing the world today is to achieve sufficient supplies covering its future demand for clean energy. Renewable energy provides a growing and vital contribution to developing countries. The proper implementation of renewable energy sources in developing countries could reduce their dependence on natural gas and oil, and investments in renewable energy technologies would be more cost-effective than fossil fuels. Nowadays, geothermal and solar energies are considered very attractive because of their world's huge resources and their important *electrical production capacity*. Geothermal power may be combined with solar energy to harness the advantages of both technologies. There are several methods of hybridizing solar and geothermal technologies, and the viability of certain methods depends on factors such as location, relative geothermal

and solar resource quality. There is a wide variety of solar energy systems. Over the years, solar chimneys attracted notable attention. This system which is more appropriate to arid and semi-arid areas is an advanced way to generate electricity from solar radiation. According to the literature, several prototypes with different scales have been constructed. The first prototype was actually placed and checked in Manzanares (Spanish town 150 km from Madrid) under the direction of German engineer Jörg Schlaich, and with funding from the German Ministry research and technology [1, 2].

The operation of such a plant is strongly dependent on the amount of solar radiation. Among all solar energy technologies, Solar chimneys are attracting special interest since they are able to operate during the day and night time [3]. The main disadvantage of this plant is that it is unable to work continuously at night. Numerous studies suggested different solutions to guarantee a continuous operation during night hours. The release of thermal energy stored during the day in the ground and/or in water tanks can overcome the disturbance of power production. This guarantees that the solar chimney is operational even at night [4]. For this reason, the Engineer Jörg Schlaich proposed additional heat storage mediums to improve the storage capacity and enable the functioning of the plant during the night. The proposed solution is to lay taught water-filled pipes underneath the collector cover. The water is heated during the day and releases this heat during nighttime [1]. In order to improve the heat storage capacity, Kreetz introduced a proposition to place water-filled tubes/tanks under the collector cover [5]. Pretorius suggested the use of a secondary collector roof to enhance the performance of the plant at night [6]. The combination of a *salt-gradient solar pond with the solar collector* was investigated by Zhou et al. The goal of this alternative is a continuous night operation for solar chimney power system [7]. To enhance the plant and ensure uninterruptible power generation, Al-Kayiem et al. proposed a new approach based on coupling the updraft tower with an exhaust heat source. The aim of this technique was to use wasted flue-gas to supply air underneath the collector [8]. Some researchers focused on enhancing the ground under the collector and employing it as storage layer [9–13]. Others suggested and investigated the usage of closed water-filled tanks [14–16]. Another alternative is proposed by Zubir et al. They suggested a *waste heat energy recovery system* based on passing the flue gases through conduits inside the collector [17]. The integration of a solar chimney power plant with another source of heat has been proposed to build a day and night functional integrated hybrid system. This proposal aims to improve the plant performance and overcome the absence of solar energy during night and cloudy days [18].

Various alternatives were proposed and investigated to enhance the performance of the solar chimney but still insufficient to allow a continuous operation of the system. Recently, some researchers introduced a novel approach to improve the solar chimney performance by hybridizing the solar plant and geothermal energy system. Reference [18] proposed a hybrid solar chimney to improve power production during the day, cloudy days, or during nighttime. The main target of this novel design is to exploit underground pipes supplied by low-temperature geothermal water to heat the

air underneath the collector and at the same time employing the PV thermal panels to produce electric energy by sunlight besides solar chimney power generation.

Other few studies suggested the integration of geothermal water tubes as heating equipment. Cao et al. studied the performance of the geothermal-solar chimney having the same Manzanares prototype dimensions. The authors compared three operational modes: the solar mode, the geothermal mode and the hybrid geothermal–solar mode [19]. The authors suggested the use of water tubes as heating device. They indicated that introducing geothermal water makes greater contribution and can achieve a 24 h-operation. To attain uninterrupted power production and enhance the energy generation of the solar chimney, Dhahri et al. considered a novel heating technique to supplement the energy input by the use of geothermal energy. A radial tubes configuration is selected for the heat exchanger. A study is conducted to examine the performance of the new hybrid power generation system for different operation modes. They concluded that by using geothermal energy, the plant would be able to deliver power during night [20].

A limited number of studies have investigated the performance of solar-geothermal chimney during nighttime. This chapter is a part of a project investigating the feasibility of coupling solar technology with geothermal energy storage to provide financially viable, reliable, and resilient energy. Existing literature has focused mainly on the daytime operation mode. The Main purpose of this work is to undertake a detailed numerical study of a hybrid solar-geothermal chimney during night based on mathematical models. The present work proposed to place an auxiliary heating system constructed of in-plane spiral coil tubes above the ground. In this chapter, a 3D numerical study was performed based on the Manzanares (Spain) prototype as a reference. Firstly, a detailed thermal model of geothermal coiled pipes is built. To evaluate the performance of the solar chimney, the mathematical models of the conventional and hybrid plants are established considering the variation of kinetic energy inside the collector. Then, the model data are validated by comparing them to Manzanares experimental measurements. To accomplish the goals of the current work, the impact of the main control parameters such as the geometric parameters and operational parameters on the novel plant performance were systematically investigated.

2 System Description and Basic Principle

2.1 Conventional Solar Chimney

A conventional solar chimney (Fig. 1) converts solar energy into electricity using three basic components: A circular collector suspended at certain height from the ground, a central chimney and a wind turbine. The Air is heated by solar radiation under the transparent collector open at the periphery. The warm air moves toward and upward into the chimney resulting from air buoyancy and difference in air pressure

Fig. 1 Conventional solar chimney power plant scheme
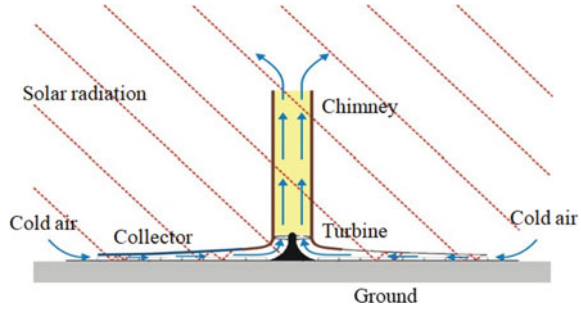
between the inside and the outside of the plant [3]. The huge pressure difference between the plant and the ambient air (chimney effect), will run the wind turbine set up at the bottom of the chimney [21]. The energy contained in the updraft air is transformed into mechanical energy by the turbine and then the generator converts it into electric energy.

The solar chimney is characterized by a 195 high chimney with a constant diameter of 10 m. the solar collector area extended to a radius of 120 m from the chimney with the glazing being 1.85 m above the ground. The turbine is housed at the bottom of the chimney [5]. The concept has been verified by constructing and successfully running a prototype in Spain for more than 6 years [22].

2.2 Hybrid Power Plant

Heating air underneath the collector is needed during the night. Therefore, it is necessary to place auxiliary heating equipment. The heat supply by geothermal energy can overcome the deficits of sunshine in the absence of solar radiation (during night hours). Arid areas of Tunisia have important resources of geothermal water. The range of water temperature in southern Tunisia is between 65 and 80 °C [23]. Different techniques can be used for air heating. One of the most appropriate and advantageous heating system is the air-soil heating system with heat pipes placed on the soil. The most used and known is heating systems with pipes above the ground. In this study, the heating is ensured via spiral pipes lying on the ground. The winding of the tube leads to obtain the body of the exchanger. The material chosen for its construction is PVC. The heating system is composed of poly-circular tube arranged on the collector floor allows by exploiting the heat from the geothermal water to heat the air entering from the periphery of the collector. This system is connected to a main supply reservoir placed near the location of the geothermal well. The exploited well is situated in the center of the plant.

The operation of the hybrid power plant is simple. The air flows from the periphery (outermost turn) to the center of the collector. Water enters the inner turn located in the center of the collector with a hot temperature and exit at the end of the spiral tube

Fig. 2 Schematic diagram of a solar chimney coupled with a spiral exchanger
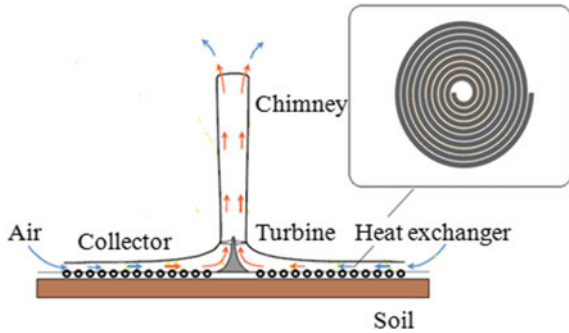
with a cooler temperature. The hot air passes from the solar collector to chimney base and moves up to the top of the chimney. It is important to keep in mind that the outlet temperature of the geothermal water should be as low as possible. Thus, the mode of circulation of the two fluids (air and water) is cross flow (Fig. 2).

The radius of the reservoir is equal to 15 m. The space between turns was fixed at 0.2 m. The distribution of heat is considered uniform, leading to neglect local heating heterogeneities along the radius of collector.

The heat exchanger design with its main geometric parameters is presented in Fig. 3. Moreover, its dimensions are illustrated in Table 1. This exchanger can be characterized by the diameter of its tube (d), the evolution of its radius of curvature (R_i) and the pitch between consecutive turns (b). These indications are sufficient to deduce the total length of the wound tube. A constant step between two consecutive turns is guaranteed. But, the curvature radius is inconstant. Other indications may be useful to complete the geometrical characterization: the radius (internal and/or external) of the tube and the tube thickness. There could be several turns, but it is limited by the flow developed in the tube.

Fig. 3 Schematic diagram of a spiral exchanger
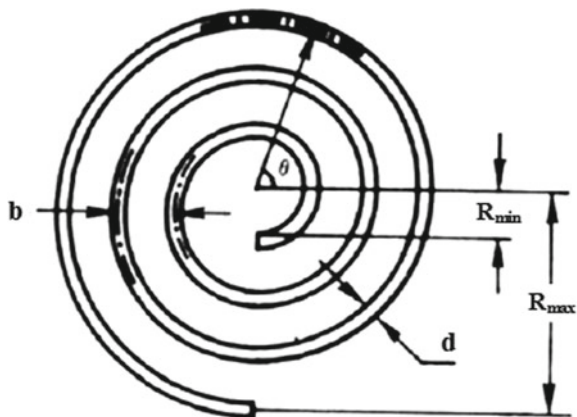
Table 1 Main dimensions

Description	Value	Unit
Tube diameter	0.2	m
Water flowrate	85.6	Kg/s
Pitch between tow turns	0.2	m
Interior radius	5	m
External radius	120	m
Turn number	92	
Inlet water temperature	70	°C

3   Thermal Modeling of the Heat Exchanger

Coiled tubes are used *commonly* in heat exchanger equipments thanks to the improved
heat transfer rate resulting from secondary flows [24]. On closer inspection, higher
temperature gradient is detected close to the external wall of the coiled tubes,
indicating a higher transfer rate.

This is mostly contributed by the secondary flow which is induced by centrifugal
forces due to the curvature of the coil [25]. As such, coiled tubing has attracted
particular attention from researchers around the world.

In the case of spiral tubes, the problem is complex because the outlet temperatures
vary depending on the position of the fluid in the exchanger. Theoretical energy
equations are expressed for a turn of the coil. In the theoretical model, each turn of
the heat exchanger is supposed to be a linear spiral. R_i and R_o are the inlet and outlet
coil radius, respectively. α represents the rate of change of the radius [24, 26].

In addition, each full rotation (2π) is approximately considered circular. The mean
radius of i-th turn, R_{mi}, is defined as:

$$R_{mi} = \frac{1}{2\pi} \int_{0}^{2\pi} R d\theta \tag{1}$$

$$R_{mi} = R_o + (2i - 1)\alpha\pi \tag{2}$$

The outlet heat transfer area (A_i) of i-th turn is expressed as follow:

$$A_i = 2\pi R_{mi} A_0 \tag{3}$$

The energy balance equation obtained for a small control volume in i-th turn is
given by:

$$\dot{m}_w C_{p,w} dT_w = U_i A_0 [T_{air} - T_w(x)] dx \tag{4}$$

The integration of (4) leads to the expression:

$$\left[T_{\text{air},i} - T_{w,i+1}\right]/\left[T_{\text{air},i} - T_{w,i}\right] = Exp(\lambda_i) \tag{5}$$

where

$$\lambda_i = (A_i U_i)/\left(\dot{m}_w C_{p,w}\right) \tag{6}$$

The equation of global energy balance developed for the i-th turn leads to:

$$\dot{m}_w C_{p,w}\left[T_{w,i} - T_{w,i+1}\right] = \dot{m}_{air} C_{p,\text{air}}\left[T_{\text{air},i} - T_{\text{air},i+1}\right] \tag{7}$$

where

$T_{air,i}$ air temperature across the i-th turn, °C
$T_{air,i+1}$ air temperature across the i + 1-th turn, °C

$$\dot{m}_{\text{air}} C_{p,\text{air}}\left[T_{\text{air},i} - T_{\text{air},i+1}\right] = \dot{m}_w C_{p,w}\left[T_{\text{air},i} - T_{w,i}\right][Exp(\lambda_i) - 1] \tag{8}$$

The approach considered in this section is to separate the geothermal heat exchanger in a sufficient number of portions. The water temperature along a plane spiral coil tube ($T_{w,\,i+1}$) is calculated iteratively from the air temperature in the vicinity of the coil, the temperature ($T_{w,\,i}$) and the heat flow rate in the preceding turn (Fig. 4). In order to determine the heat transported by geothermal water to the indoor air, the water outlet temperature is required. For this reason, an iterative calculation based on (7) and (8) must be conducted to calculate this temperature at the exit of each turn for a given inlet temperature.

The amount of heat transported by the hot water along the pipe is evaluated by:

$$\dot{Q}_{\text{geoth}} = \dot{m}_w C_{p,w}\left(T_{w,e} - T_{w,s}\right) \tag{9}$$

Fig. 4 Descriptive diagram of a spiral exchanger
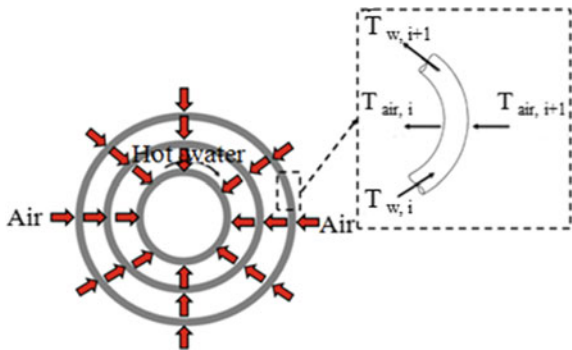
4 Mathematical Model

The most important element of a solar chimney system is the collector. In this section, a complete theoretical model is *developed* to investigate the thermal collector performance. Both conventional and hybrid solar chimney power plant are considered in this section.

4.1 Conventional Solar Chimney

We propose to take into account the kinetic energy variation in the collector energy equation. A new term is introduced in the global energy balance of the collector. When relevant literature in solar chimney systems is reviewed, it is seen that the researchers had not considered kinetic energy term in their mathematical models. The energy balance in this case may be written as follows [20, 27]:

$$0 = \dot{Q}_s - \dot{Q}_p + \rho_1 A_1 V_1 \left(C_{p,a} T_1 + \frac{V_1^2}{2} \right) - \rho_2 A_2 V_2 \left(C_{p,a} T_2 + \frac{V_2^2}{2} \right) \qquad (10)$$

The *Convective heat loss* from the collector to the environment is expressed as:

$$\dot{Q}_p = U_p A_{\text{coll}} (T_{\text{air},i} - T_{\text{amb}}) \qquad (11)$$

Where A_1, A_2 et A_{coll} are expressed respectively by: $A_1 = 2\pi R h_{\text{coll}}$, $A_2 = 2\pi r h_{\text{coll}}$ and $A_{\text{coll}} = \pi R^2$.

The air outlet velocity of the solar collector can be calculated using the following relation:

$$V_2 = \sqrt{\sqrt[3]{-\frac{q}{2} - \frac{1}{2}\sqrt{\frac{27q^2 + 4p^3}{27}}} + \sqrt[3]{-\frac{q}{2} + \frac{1}{2}\sqrt{\frac{27q^2 + 4p^3}{27}}}} \qquad (12)$$

Where

$$p = 2 C_p T_2 \qquad (13)$$

$$q = -\frac{2G}{\rho_{\text{coll}} A_2} + \frac{2 h_{\text{conv}} A_{\text{coll}} (T_c - T_{\text{air}})}{\rho_{\text{coll}} A_2} - 2 V_1 \frac{A_1}{A_2} \left(C_p T_1 + \frac{V_1^2}{2} \right). \qquad (14)$$

4.2 Hybrid Geothermal-Solar Chimney

The main restriction in renewable energy plants lies in the interrupted nature of the energy source and the requirement of a site with specific nature. But this restriction can frequently be surmounted with a combination of technologies. Since the sun is not available during nighttime and overcast days, we proposed to combine the solar chimney with an auxiliary heating system to guarantee a 24 h continuous operation. The current *research study focus is* on modeling the night mode of a geothermal-solar chimney with assumption of absence of solar radiation on the plant.

4.2.1 Thermal Heat Losses at the Collector

To carry out an energy equation on a solar collector, thermal losses associated with the collector should be evaluated for a given heat energy flow. The cover acts as an intermediary *between the collector zone* and the outdoor *environment*. The major collector heat losses are from the front roof. The heat transfer by natural convection between the interior air and the internal wall of the canopy is given by following equation [20].

$$\dot{Q}_{p,i} = h_i A_{coll}(T_{air,i} - T_c) \tag{15}$$

h_i is the convective heat transfer coefficient between the inside air and the inner face of the collector. h_i can be calculated by [20]:

$$h_i = \left[0.2106 + 0.0026v \left(\frac{\rho T_m}{\mu g \Delta T} \right)^{1/3} \right] \Big/ \left[\frac{\mu T_m}{g \Delta T c_p \lambda^2 \rho^2} \right]^{1/3} \tag{16}$$

Air properties including:density, thermal conductivity, dynamic viscosity and heat capacity are estimated at the average temperature. The air properties can be obtained based on (17–20) at temperatures varying between 300 and 350 K [20].

$$\rho = 1.1614 - 0.00353(T - 300) \tag{17}$$

$$\lambda = 0.0263 + 0.000074(T - 300) \tag{18}$$

$$\mu = [1.846 + 0.00472(T - 300)] \times 10^{-5} \tag{19}$$

$$C_p = [1.007 + 0.00004(T - 300)] \times 10^3 \tag{20}$$

The convective heat loss through the external face of the collector roof can be expressed as follows:

$$\dot{Q}_{p,e} = h_e A_{\text{coll}}(T_c - T_{\text{air},e}) \tag{21}$$

The correlation of McAdams is employed to evaluate the external convective heat transfer coefficient [20]:

$$h_e = 5.67 + 3.86 v_{\text{amb}} \tag{22}$$

The main role of the heat exchanger is to supply energy to *equalize* the heat losses taking place during periods when the indoor air temperature overpasses the outdoor temperature.

Analytical models generally include some simplifying presumptions that make the problem manageable. The soil beneath the collector cover acts as a storage medium. To facilitate numerical calculations, the energy stored up in the soil during daytime periods and released during nighttime will be neglected in this study. Comparing the heating technique (water tubes) with the ground, showed that the heat exchange between water pipes and water is much greater than that of soil surface and layers located beneath since the water heat capacity is almost five times superior than that of ground [28, 29]. Energy losses at the level of the collector cover will be neglected in our calculations and are considered equal to zero. The collector energy equation is represented by the expression (23).

$$\frac{\dot{m}_w C_{p,w}}{\rho_{\text{coll}} A_2}(T_{w,e} - T_{w,s}) + \frac{A_1}{A_2}\left(C_{p,a} V_1 T_1 + \frac{V_1^3}{2}\right) = C_{p,a} V_2 T_2 + \frac{V_2^3}{2} \tag{23}$$

4.2.2 Outlet Air Velocity (not Including Thermal Losses)

Rearranging (23) led to the equation below:

$$V_2^3 + 2C_{p,a} V_2 T_2 - \frac{2\dot{m}_w C_{p,w}}{\rho_{\text{coll}} A_2}(T_{w,e} - T_{w,s}) - 2\frac{A_1}{A_2}\left(C_{p,a} V_1 T_1 + \frac{V_1^3}{2}\right) = 0 \tag{24}$$

By solving (24), we find the formula of the outlet air velocity. This solution has the form:

$$V_2 = \sqrt[3]{-\frac{q}{2} - \frac{1}{2}\sqrt{\frac{27q^2 + 4p^3}{27}}} + \sqrt[3]{-\frac{q}{2} + \frac{1}{2}\sqrt{\frac{27q^2 + 4p^3}{27}}} \tag{25}$$

where

$$p = 2C_{p,a} T_2 \tag{26}$$

$$q = -\frac{2\dot{m}_w C_{p,w}}{\rho_{\text{coll}} A_2}\left(T_{w,e} - T_{w,s}\right) - 2\frac{A_1}{A_2}\left(C_{p,a}V_1 T_1 + \frac{V_1^3}{2}\right) \tag{27}$$

4.2.3 Outlet Air Velocity (with Thermal Losses)

In this part, the thermal losses of the collector are considered. The collector heat balance with inclusion of thermal heat losses is expressed by:

$$\frac{\dot{m}_w C_{p,w}}{\rho_{\text{coll}} A_2}\left(T_{w,e} - T_{w,s}\right) + \frac{A_1}{A_2}\left(C_{p,a}V_1 T_1 + \frac{V_1^3}{2}\right)$$
$$-\frac{U_p A_{\text{coll}}}{\rho_{\text{coll}} A_2}(T_{\text{air},i} - T_{\text{amb}}) = C_{p,a}V_2 T_2 + \frac{V_2^3}{2} \tag{28}$$

$$V_2^3 + 2C_{p,a}V_2 T_2 - \frac{2\dot{m}_w C_{p,w}}{\rho_{\text{coll}} A_2}\left(T_{w,e} - T_{w,s}\right) - 2\frac{A_1}{A_2}\left(C_{p,a}V_1 T_1 + \frac{V_1^3}{2}\right)$$
$$+\frac{2U_p A_{\text{coll}}}{\rho_{\text{coll}} A_2}(T_{\text{air},i} - T_{\text{amb}}) = 0 \tag{29}$$

The resolution of (29) conducts to the find out of the outlet air velocity.

5 Numerical Approach and Boundary Conditions

In the presented study, a finite volume method was applied to resolve the governing equations using the CFD software FLUENT. The pre-processor software GAMBIT was employed for creating mesh, assigning boundary conditions and determining the computational domain. The computational domain is illustrated in Fig. 5. The mesh quality can be *better controlled* with geometric splitting process. In this study, the whole computational domain is partitioned into *multiple* sub-domains (collector, transition part, and chimney), each of which is meshed independently. The part with extremely elevated pressure gradients necessitates a *fine grid* resolution. Therefore, the tetrahedral meshes were used in the transition section. The two other sub-regions are meshed with hexahedral elements [27].

After grid independence study, it was noticed that a mesh with 1,228,452 cells is adequate for numerical analysis (Fig. 5). The numerical simulation of turbulent flow is performed for 3D case of a solar chimney plant. During simulation, the turbulence model k-ε standard was used.

The solver pressure-based is specified in ANSYS Fluent. The SIMPLE scheme is used for velocity-pressure coupling [27]. The relaxation factors were as follows: pressure = 0.3, velocity = 0.7, energy = 1 and radiation = 1. A second order upwind scheme was applied for *discretization* of the velocity and temperature fields, while the

Fig. 5 Numerical grid
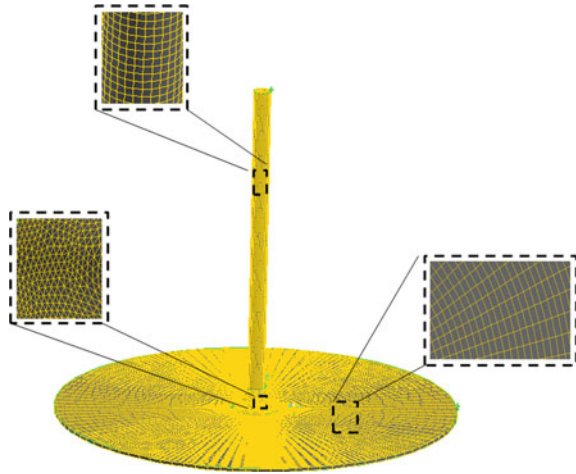
PRESTO *discretization* scheme was used for pressure field. The Discrete Ordinate (*DO*) *model* is used for *radiation.* In this study, the Discrete Ordinate (*DO*) *model* is used to compute *radiation.* This model is appropriate to solve the radiation through a semi-transparent medium.

For residuals of continuity and momentum equations, a convergence criterion of 10^{-3} was required while 10^{-6} as energy and radiation equations residuals.

6   Results and Discussions

This section presents the results of the numerical simulation under different geometrical and operational conditions. Several key parameters affecting flow behavior and heat transfer performance have been evaluated and examined. Four main parameters used in the parametric study, namely, the effect of collector radius, coil pitch, tube diameter and water inlet temperature are investigated in details.

6.1   Validation

The validation is performed by comparing the CFD results with experimental data from the Spanish prototype. The previous *measurements are taken* on September 1982. The calculation results and the experimental data are illustrated in Table 2. We conclude that our calculated values have shown close agreement with the experimental data from the Spanish plant.

The air exit velocity were calculated and presented in Fig. 6 for several solar irradiation values varying between 100 and 1000 W/m^2. The examination of Fig. 6

Table 2 Comparison between numerical and experimental results

Solar radiation (W/m^2)		Numerical data	Experimental data
800	ΔT (°C)	17.783	17
1000	ΔT (°C)	19.277	20

Fig. 6 Effect of solar radiation on outlet air velocity
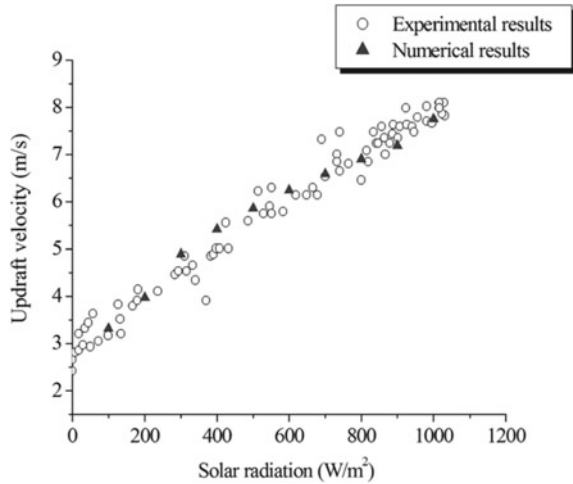
shows that the numerical data are in a satisfactory agreement with the experimental measurements [27]. The small difference between the calculated and experimentally obtained data at the outlet of the collector corroborates the validity of the results.

6.2 The Impact of Collector Radius on the Plant Performance

The collector radius is an *important* factor that greatly influences the solar plant performance. To investigate the impact of the collector radius on the hybrid plant performance, different values of radius were considered (40, 60, 80, 100, 120 and 140 m) and main dimensions of the prototype are kept constant apart from the radius of the collector. Figure 7 displays the distribution of outlet air velocity against the collector radius. A constant water temperature equal to 70 °C was considered. In this section, the study is carried out for a given total water flow rate (85.6 kg/s).

These results highlight a marked influence of the collector radius. After various numerical tests, it was found that *during* the *night*, the collector exit air velocity drop significantly as the radius increases.

Fig. 7 Air velocity variation
against collector radius
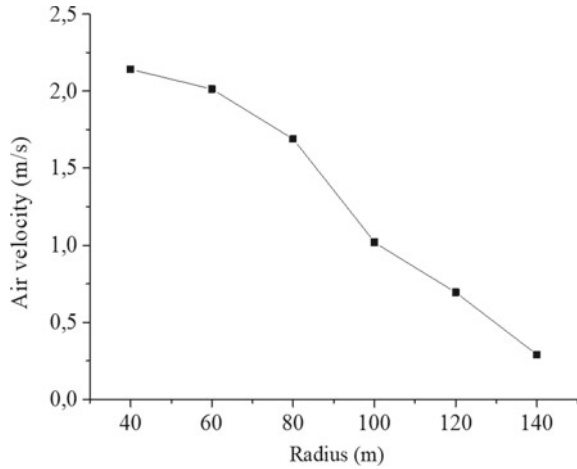
6.3 Investigation of Coil Pitch

Spacing plays an essential role in the design of spiral heat exchangers. The analyses of
the heat flow rate for different coil pitch are important. Tests have been made to study
the effect of the variation of the spacing between consecutive turns on the amount of
heat exchanged between the geothermal water and the air circulating underneath the
collector. Figure 8 shows the change in heat flow rate for different spacing between
the spiral turns.

We chose to vary the pitch between 0.2 and 1 m. Note that increasing the pitch leads
to a reduction of the number of turns which varies from 92 to 19. For a pitch ranging
from 0.2 to 0.4 m, it can be seen that rising the pitch coil induces the augmentation of
heat transfer rate. Apparently, the in-plane spiral heat exchanger has a smaller mean

Fig. 8 Variation of heat flow
rate against the coil pitch
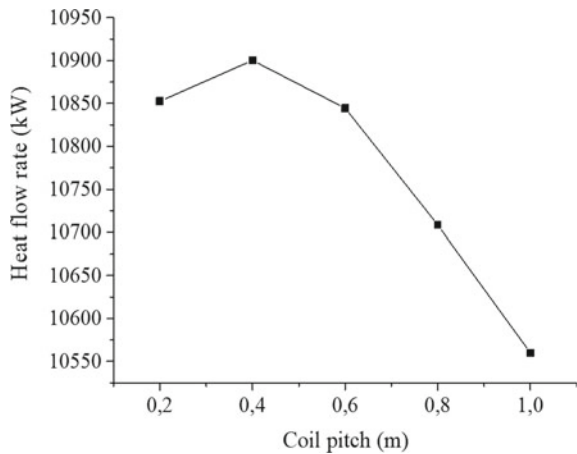
bend radius and a shorter tube length for a bigger coil pitch. Small curve radius is advantageous to the heat exchange process. Therefore, the heat flux rises with the increment of the coil pitch.

Beyond these values, a dramatic change in the heat flow rate is observed. The increase in the coil pitch will result in a lower amount of heat. The calculated data show clearly the influence of the pitch variation on the performance of the spiral heat exchanger. So maintaining a constant pitch is one of the key parameters that guarantee a good performance. In addition, it is necessary to maintain a sufficient spacing so that air can circulate easily between the tubes.

6.4 Investigation of Tube Diameter

The Fig. 9 shows the variation of the geothermal heat flux against the tube diameter. Nine cases were considered to evaluate the impact of the tube diameter on the heat flux by varying the diameter from 0.2 to 1 m. In addition, the water flow rate, the coil pitch and the collector size are assumed to be constant.

It can be seen that the increase in tube diameter can significantly affect the rate of heat transferred to the internal air. For a diameter value less than 0.4 m, the heating capacity increases. It should be noted that beyond this value, the heat flow recovered from the hot water decreases. This may be due to the reduction of the effect of centrifugal force (as a result of the pipe curve). This leads ultimately to the reduction of the secondary flow (Dean Effect) for largest coil diameter. The intensity of the secondary flow created in the pipe is dependent on coil geometry and pipe diameter [30–33].

Fig. 9 Heat flow rate variation versus tube diameter
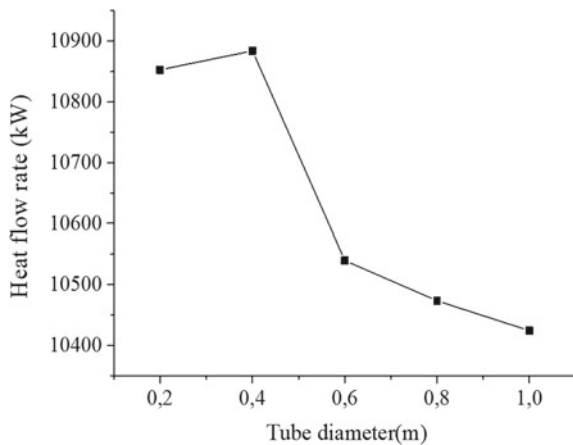
6.5   Geothermal Water Flow Investigation

With the aim of examining the impact of the indoor water flow rate on the thermal performance of the coiled tube heat exchanger, a study is performed assuming a constant geothermal water temperature (70 °C) and for a constant collector radius (120 m).

The constructional parameters of the heat exchanger are held fixed values ($R_i =$ 5 m, $R_0 = 120$ m, $b = 0.2$ m, $d = 0.2$ m). Figure 10 displays the variation of the amount of heat in terms of the water flow along the spiral coil pipes. The flow rates of water considered are in the 85.6- 214 kg/s range.

As expected, we can notice in Fig. 10 that it is advantageous to increase the total flow of geothermal water. All calculations were made with the same geometrical parameters of Manzanares prototype. A total of 7 cases were considered in this study by varying the flow rate with an increment of 21.4 kg/s. The bigger the water flow rate, the greater the amount of heat recovered by the air passing through the collector. The Fig. 10 also confirms that it is preferable to increase the water inlet flow rate to obtain higher air velocities.

6.6   Effect of Water Inlet Temperature

To evaluate the impact of varying inlet water temperature on heat flow rate, the numerical tests are performed for a water temperature in the range of 55–75 °C.
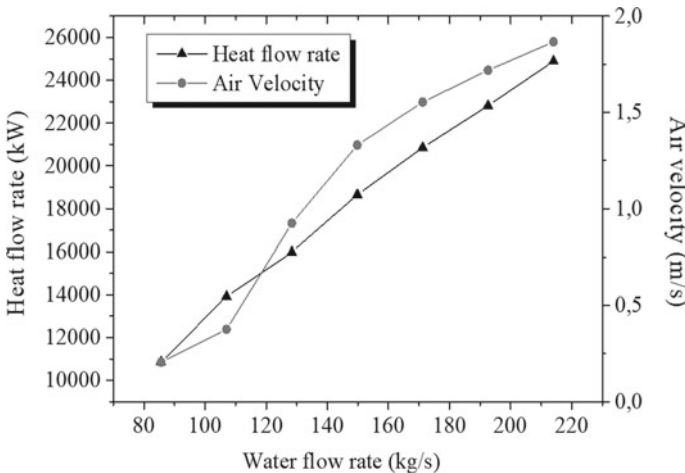
Fig. 10 Effect of water flow rate

Fig. 11 Heat Flow rate as a function of water inlet temperature
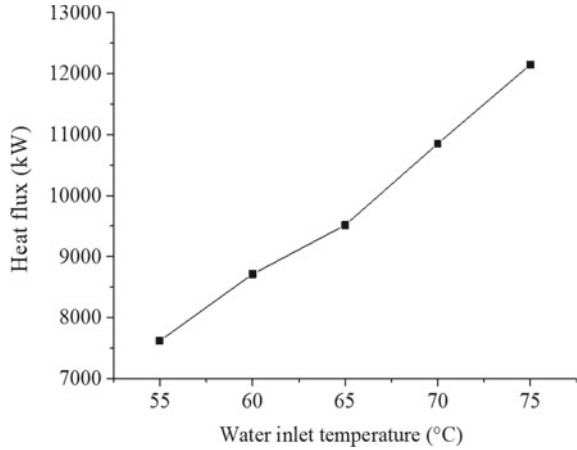
The value of geothermal water flow is kept to be constant (85.6 kg/s). Except the water inlet temperature, all parameters were fixed as constant values. Computational simulations were conducted for the same geometric model of the Spanish prototype. Figure 11 shows a net increase of the geothermal power and a significant effect of inlet water temperature. In addition, this figure indicates that the difference between the quantities of heat supplied by the heat exchanger can reach 12.38% on average. It can be concluded that the more the operating temperatures and input flow rate are well chosen, the more efficiently the heat exchanger will operate. The Fig. 11 shows that for a stated water mass flow rate, the overall rate of heat transfer increases with the increase of the inlet water temperature.

6.7 Variation of Internal Air and Geothermal Water Temperatures

It seems important to investigate the impact of the heater size on the temperatures of the two working fluids. To investigate the effect of collector size, we have varied the radius from 40 to 140 m. Figure 12 shows the variation of the water and air temperatures at the exit of each turn for a constant geothermal water flow. The number of turns corresponding to this case is 92. The water enters at the inlet of the tube located in the center of the collector with a hot temperature (70 °C) and comes out at the end of the spiral with a colder temperature (39 °C). According to Fig. 12, the water outlet temperature drops quickly initially, but then slows down. Thus, the air temperature near the tube is cooler on the outside and warmer inwards (radially), as it approaches the water exit temperature. This temperature increases less rapidly. As it can be seen from Fig. 12, for a number of turns equal to 40, the temperatures of the working fluids are almost stable.

Fig. 12 Variation of air and geothermal water temperatures against turn number
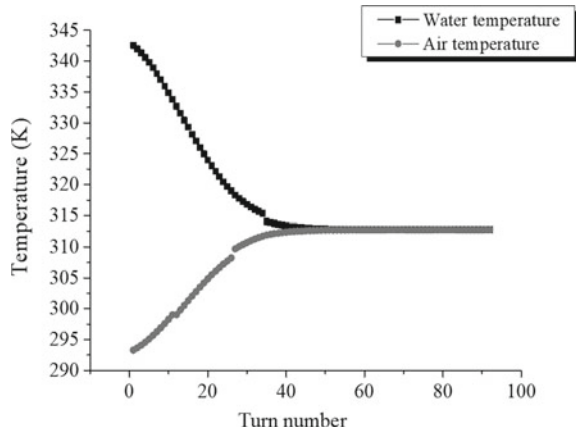
The obtained results can be related to the development of secondary flow as a result of centrifugal force. This force has long been identified as the most important feature of coiled tubes and it is created due to the pipe curvature effect [34]. Heat Transfer associated with spiral ducts is more difficult than that occurring in straight pipes. This difference depends on the occurrence of secondary flows caused by centrifugal forces that considerably influence the heat and mass transfer. It is also interesting to note that stronger secondary flow intensity results in greater rates of heat transfer. But the increase in heat transfer is more marked in the laminar regime. Since the regime flow considered in this study is turbulent, the increase in heat transfer is less important than in the case of laminar flow [35]. Turbulence effects dominate over secondary high Reynolds flow, making the heat transfer coefficient equivalent to straight tubes [36]. The secondary flow is found to have a considerable influence on the evolution of temperature profiles and flow rate in the spiral duct [37].

6.8   Collector Heat Losses

To examine the impact of radius variation on heat dissipation rate in the collector, the radius was varying from 40 to 140 m. It should be noted that for a radius less than 80 m, any augmentation of the radius induces the increase of the collector energy losses (Fig. 13). In the case of a radius equal to 100 m, the lower energy losses are mainly due to the decrease of convective losses in the outer surface of the collector cover. Exceeding 120 m, the temperature of indoor air is lower than the outside air. A temperature inversion appears and convective exchange from the cover to the outside air in the opposite direction is observed. This phenomenon occurs when thermal losses through the cover are very high and the cover temperature may drop several degrees below the outside air temperature.

Fig. 13 Collector heat
losses as a function of radius
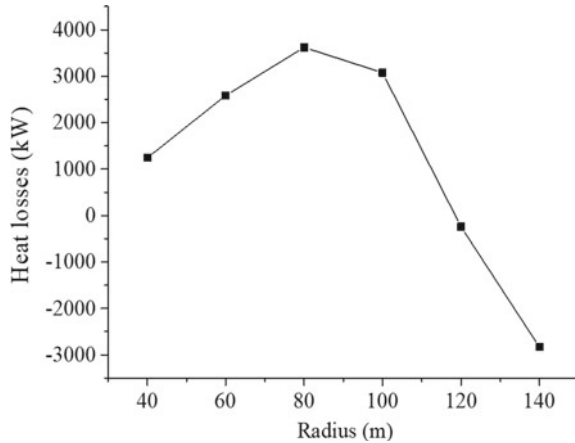
7 Conclusion

A computational study was conducted to examine the night operation of a solar
chimney combined to a spiral heat exchanger. The use of geothermal water is an
advantageous solution due to its ability to ensure a continuous operation of the plant
by fulfilling the nocturnal power demand. This work has identified the parameters
affecting the system performance overnight. The Analysis of the combined system
behavior leads to the following findings:

1. The air exit velocity at night depends strongly on the size of the collector.
2. The use of geothermal energy may improve the performance of the solar chimney
   overnight.
3. The geometrical dimensions of the heating device (coil pitch and tube diameter)
   have a prominent impact on the heat transfer process.
4. The rate of heat transferred *to the interior air* is greatly determined by the
   exchanger operational parameters (inner temperature and water flow rate). The
   higher these parameters, the greater the collector outlet air velocity.
5. *Canopy thermal losses* increase notably once the collector radius is beyond 80 m.
   for a radius exceeding 120 m, a temperature inversion phenomenon appears and
   convective exchange from the cover to the outside air in the opposite direction is
   observed.

References

1. Schlaich J (1995) The solar chimney: electricity from the, sun edn. Axel Menges, Felbach
2. Goswami DY, Zhao Y (2009) Proceedings of ISES world congress 2007, vol 1–vol 5. Solar energy and human settlement. Springer Science & Business Media
3. Chikere AO, Al-Kayiem HH, Karim ZAA (2011) Review on the enhancement techniques and introduction of an alternate enhancement technique of solar chimney power plant. J Appl Sci 11(11):1877–1884
4. Fasel HF, Meng F, Shams E, Gross A (2013) CFD analysis for solar chimney power plants. Solar Energy Part A 98:12–22
5. Kreetz H (1997) Theoretische Untersuchungen und Auslegung eines temporärenWasserspeichers für das Aufwindkraftwerk, dissertation, Technical University Berlin
6. Fathi N, McDaniel P, Aleyasin SS, Robinson M, Vorobieff P, Rodriguez S, de Oliveira C (2018) Efficiency enhancement of solar chimney power plant by use of waste heat from nuclear power plant. J Clean Prod 180:407–416
7. Kasaeian AB, Molana S, Rahmani K et al (2017) A review on solar chimney systems. Renew Sustain Energy Rev 67:954–987
8. Al-Kayiem HH et al (2019) Performance evaluation of hybrid solar chimney for uninterrupted power generation. Energy 166:490–505
9. Hurtado FJ, Kaiser AS, Zamora B (2012) Evaluation of the influence of soil thermal inertia on the performance of a solar chimney power plant. Energy 47(1):213–224
10. Zheng Y, Ming TZ, Zhou Z, Yu XF, Wang HY, Pan Y, Liu W (2010) Unsteady numerical simulation of solar chimney power plant system with energy storage layer. J Energy Inst 83(2):86–92
11. Ming TZ, Zheng Y, Liu W, Huang XM (2009) Unsteady numerical conjugate simulation of the solar chimney power generation systems. J Eng Thermophys 30:4
12. Fanlong M, Tingzhen M, Yuan P (2011) A method of decreasing power output fluctuation of solar chimney power generating systems. In: 2011 3rd international conference on measuring technology and mechatronics automation (ICMTMA), vol 1, pp 114–118
13. Yan Zhou XHL (2011) Unsteady conjugate numerical simulation of the solar chimney power plant system with vertical heat collector. Mater Sci Forum 704–705:535–540
14. Robert AL, Craig RB, Eckhard AG et al (2012) Alternative heat rejection methods for power plants. Appl Energy 92:17–25
15. Barbier E (2002) Geothermal energy technology and current status: an overview. Renew Sustain Energy Rev 6(1–2):3–65
16. Al-Kayiem HH, Brebbia CA, Zubir SS (2014) Energy and sustainability V. WIT Press, UK
17. Zubir SS, Brebbia A (2013) The sustainable city VIII (2 volume set): urban regeneration and sustainability. WIT Press, UK
18. Aurybi MA, Al-Kayiem HH, Gilani SIU, Ismaeel AA (2017) Numerical analysis of solar updraft power plant integrated with external heat source. In: UTP-UMP symposium on energy systems 2017 (SES 2017), vol 131, (MATEC Web Conf.), pp 7
19. Cao F, Li H, Ma Q, Zhao L (2014) Design and simulation of a geothermal–solar combined chimney power plant. Energy Convers Manag 84:186–195
20. Dhahri A, Omri A, Orfi J (2018) Theoretical analysis of the performance of a solar chimney coupled with a geothermal heat exchanger. In: Driss Z, Necib B, Zhang HC (eds) CFD techniques and energy applications. Springer, Cham
21. Elmagid WMA, Kepple I (2017) Axial flow turbine for solar chimney. Hung Agric Eng J 32:29–37
22. Weinrebe G, Bergermann R, Schlaich J (2012) solar updraft towers. In: Meyers RA (ed) Encyclopedia of sustainability science and technology. Springer, New York, NY
23. Verlodt H (1983) Amélioration du bilan thermique sous abri-serre. Tropicultura 1(2):59–69
24. Ho JC, Wijeysundera NE (1996) Study of a compact spiral-coil cooling and dehu midifying heat exchanger. Appl Therm Eng 16(10):777–790

25. Nguyen DK, San JY (2016) Heat transfer and exergy analysis of a spiral heat exchanger. Heat Trans Eng 37(12):1013–1026
26. Wijeysundera NE, Ho JC, Rajasekar S (1996) The effectiveness of a spiral coil heat exchanger. Int Commun Heat Mass Transfer 23(5):623–631
27. Dhahri A, Omri A, Orfi J (2014) Numerical study of a solar chimney power plant. Res J Appl Sci Eng Technol 8:1953–1965
28. Cuce E, Cuce PM (2019) Performance assessment of solar chimneys: part i–impact of chimney height on power output. Energy Res J 10:11–19
29. Bernardes MAdS (2004) Technische, ökonomische und ökologische Analyse von Aufwindkraftwerken, Ph.D. Thesis. Universität Stuttgart
30. Deshpande M et al (2012) Study of hydrodynamics of horizontal spiral coil tube. Int J Adv Eng Res Stud 1(3):112–114
31. Purandare PS, Lel MM, Gupta R (2012) Parametric analysis of helical coil heat exchanger. Int J of Eng Res Technol 1(8)
32. Mukesh Kumar PC, Chandrasekar M (2019) CFD analysis on heat and flow characteristics of double helically coiled tube heat exchanger handling MWCNT/water nanofluids. Heliyon 5(7):e02030
33. Chaware P, Sewatkar CM (2018) Effects of tangential and radial velocity on fluid flow and heat transfer for flow through a pipe with twisted tape insert—laminar flow. Sādhanā 43(9):1
34. Yoo G, Choi H, Dong W (2012) Fluid flow and heat transfer characteristics of spiral coiled tube: effects of reynolds number and curvature ratio. J Cent South Univ Technol 19:471–476
35. Bergman TL, Incropera FP (2011) Introduction to heat transfer. John Wiley & Sons
36. Pablo Coronel KPS (2008) Heat transfer coefficient in helical heat exchangers under turbulent flow conditions. Int Jof Food Eng 4(1)
37. Naphon P, Suwagrai J (2007) Effect of curvature ratios on the heat transfer and flow developments in the horizontal spirally coiled tubes. Int J Heat Mass Transfer 50:444–451